

Sonolytic Hydrolysis of *p*-Nitrophenyl Acetate: The Role of Supercritical Water

Inez Hua, Ralf H. Höchemer, and Michael R. Hoffmann*

W. M. Keck Laboratories, California Institute of Technology, Pasadena, California 91125

Received: July 12, 1994; In Final Form: September 30, 1994[⊗]

Ultrasonic irradiation is shown to accelerate the rate of hydrolysis of *p*-nitrophenyl acetate (PNPA) in aqueous solution by 2 orders of magnitude over the pH range of 3–8. In the presence of ultrasound, the observed first-order rate constant for the hydrolysis of PNPA is found to be independent of pH and ionic strength with $k_{\text{obs}} = 7.5 \times 10^{-4} \text{ s}^{-1}$ with Kr as the cavitating gas, $k_{\text{obs}} = 4.6 \times 10^{-4} \text{ s}^{-1}$ with Ar as the cavitating gas, and $k_{\text{obs}} = 1.2 \times 10^{-4} \text{ s}^{-1}$ with He as the cavitating gas. The apparent activation parameters for sonolytic catalysis are $\Delta H^\ddagger(\text{sonified}) = 211 \text{ kJ/mol}$, $\Delta S^\ddagger(\text{sonified}) = -47 \text{ J/(mol K)}$, and $\Delta G^\ddagger(\text{sonified}) = 248 \text{ kJ/mol}$. Under ambient conditions and in the absence of ultrasound, k_{obs} is a strong function of pH where $k_{\text{obs}} = k_{\text{H}_2\text{O}}[\text{H}_2\text{O}] + k_{\text{OH}^-}[\text{OH}^-]$ with $k_{\text{H}_2\text{O}} = 6.0 \times 10^{-7} \text{ s}^{-1}$ and $k_{\text{OH}^-} = 11.8 \text{ M}^{-1} \text{ s}^{-1}$ at 25 °C. The corresponding activation parameters are $\Delta H^\ddagger = 71.5 \text{ kJ/mol}$, $\Delta S^\ddagger = -107 \text{ J/(mol K)}$, and $\Delta G^\ddagger = 155 \text{ kJ/mol}$. During cavitation bubble collapse, high temperatures and pressures exceeding the critical values of water ($T > T_c = 647 \text{ K}$ and $P > P_c = 221 \text{ bar}$) occur in the vapor phase of the cavitating bubbles and at the interfaces between the hot vapors and the cooler bulk aqueous phase. The formation of transient supercritical water (SCW) appears to be an important factor in the acceleration of chemical reactions in the presence of ultrasound. The apparent activation entropy, ΔS^\ddagger , is decreased substantially during the sonolytic catalysis of PNPA hydrolysis, while ΔG^\ddagger and ΔH^\ddagger are increased. The decrease ΔS^\ddagger is attributed to differential solvation effects due to the existence of supercritical water (e.g., lower ρ and ϵ) while the increases in ΔG^\ddagger and ΔH^\ddagger are attributed to changes in the heat capacity of the water due to the formation of a transient supercritical state. A dynamic heat-transfer model for the formation, lifetime, and spatial extent of transient supercritical water at cavitating bubble interfaces is presented.

Introduction

The application of ultrasonic irradiation for the controlled degradation of chemical contaminants in water has been investigated recently using several model compounds.^{1–5} Upon the passage of ultrasonic waves, water molecules are exposed to alternative compression and rarefaction cycles. During a rarefaction cycle, the liquid density is low enough to form a cavitation bubble containing water vapor, dissolved gases, and high vapor pressure solutes. During a compression cycle, a preexisting cavity is compressed resulting in localized high temperatures and pressures. Equations describing the inception and dynamics of a cavitation bubble have been developed.^{6–8} With these equations, a theoretical temperature of 4200 K and a pressure of 975 atm have been predicted for a collapsing cavitation bubble in an aqueous solution saturated with N_2 .⁹ Experimental values of $P = 313 \text{ atm}$ and $T = 3360 \text{ K}$ have been reported.¹⁰ Cavitation temperatures in excess of 5000 K in organic and polymeric liquids have been reported.^{11,12}

Two distinct sites for chemical reaction exist during a single cavitation event.¹³ They are the gas phase in the center of a collapsing cavitation bubble and a thin shell of superheated liquid surrounding the vapor phase. The volume of the gaseous region is estimated to be larger than that of the thin liquid shell by a factor of $\sim 2 \times 10^4$ ¹⁴ in organic liquids.

Chemical transformations are initiated predominantly by pyrolysis at the bubble interface or in the gas phase, and attack by hydroxyl radicals generated from the decomposition of water. The concentration of $\cdot\text{OH}$ at a bubble interface in water has been estimated to be $4 \times 10^{-3} \text{ M}$.¹⁵ Depending on its physical properties, a molecule can simultaneously or sequentially react in both the gas and interfacial liquid regions.

p-Nitrophenol (*p*-NP) is degraded completely by sonolysis to yield short-chain carboxylic acids, CO_2 , NO_3^- , and NO_2^- .¹ Intermediate products resulting from both hydroxyl radical attack and thermal bond cleavage are detected. Hydroxyl radical attack on *p*-NP is thought to occur in a region of the bubble interface with $T < 440 \text{ K}$, while pyrolysis occurs in a hotter interfacial region with an average temperature of 900 K.¹ On the other hand, H_2S^2 appears to be degraded primarily by pyrolytic decomposition within the compressed vapor phase.

Even though the basic physical and chemical consequences of cavitation are understood, many fundamental questions about the cavitation site in aqueous solution remain unanswered. In particular, the dynamic temperature and pressure changes at the bubble interface and their effects on chemical reactions need to be explored. Since this region is likely to have transient temperatures and pressures in excess of 647 K and 221 bar for periods of microseconds to milliseconds, we propose that supercritical water (SCW) provides an additional phase for chemical reaction. This phase of water exists above the critical temperature, T_c , of 647 K and the critical pressure, P_c , of 221 bar and has physical characteristics intermediate between those of a gas and a liquid.¹⁶ The physicochemical properties of water such as viscosity, ion product, density, and heat capacity change dramatically in the supercritical region.^{16,17} These changes favor substantial increases for rates of most chemical reactions. SCW has been used in industrial applications such as extraction¹⁸ and hydrolysis^{19,20} and for environmental applications such as the destruction of hydrocarbons²¹ and phenols.^{22,23}

In this paper, we present experimental results on the kinetics of *p*-nitrophenyl acetate (*p*-NPA) hydrolysis in support of our hypothesis of the existence of transient SCW during ultrasonic irradiation in water. In addition, we present an elementary heat-

* To whom correspondence should be addressed.

[⊗] Abstract published in *Advance ACS Abstracts*, February 1, 1995.

transfer model for the estimation of the lifetime and spatial extent of supercritical water during cavitation bubble collapse.

Experimental Methods

Sonication was performed with a direct immersion-probe system (VCX-400 from Sonics and Materials). The irradiation horn was immersed reproducibly (3 cm below the surface) into the sample solution. The average power delivered to the aqueous phase was 115 W, which corresponds to an intensity of approximately 96 W/cm². Solutions of 100 μM *p*-NP were adjusted to pH 4.8–5.2 with phosphoric acid and sonolysis reactions were performed in a modified stainless-steel cell on a total volume of 25 mL. The cell was modified by the addition of stainless-steel gas dispersion and sampling tubes. A small Teflon tube with “luer-lok” connection (Aldrich) was inserted through the sampling tube. The reaction chamber was stirred with a magnetic stirring bar and stirring motor. Compressed air was blown continuously through the converter to minimize changes in temperature of the piezoelectric crystal. pH was adjusted to the range pH 4.8–5.2 to ensure that all of the *p*-NP ($pK_a = 7.16$ at $I = 0.05$ M)¹ was in the neutral form such that it would preferentially partition to the gas bubble interfaces. The reaction solution was sparged for 15 min at a flow rate of 10–15 mL/min with the appropriate gas. Constant temperature was maintained with a Haake A80 temperature control system. Aliquots of 0.5 mL were withdrawn via syringe through the sampling tube at variable time intervals. Even though the total reaction volume was not maintained constant during sonication, dV/dt was determined to be small and thus did not have an effect on the value of the measured rate constant. The pH of the sample aliquots was adjusted to ~12 with 5 N NaOH and then filtered through 0.2 μm syringe filters (PFTE, Gelman). The degradation of *p*-NP was monitored spectrophotometrically at $\lambda = 400$ nm ($\epsilon = 17\,900$ M⁻¹ cm⁻¹) with an HP8542a UV/vis spectrophotometer.

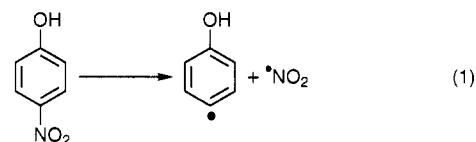
The rates of *p*-NPA hydrolysis in the absence of ultrasound were determined in a temperature-controlled optical cell using an HP8450a UV/vis spectrophotometer. The appearance of *p*-nitrophenolate ion was monitored at $\lambda = 360$ or 400 nm. *p*-NPA was dissolved in a small volume of methanol before dilution in water; and solutions were used immediately after preparation. The ionic strength was maintained at $\mu = 0.4$ M with NaCl and over the pH range of 2–11, three different buffers (i.e., CH₃COOH/CH₃COO⁻, CO₂·H₂O/CO₃²⁻; HCO₃⁻/CO₃²⁻) and concentrations were used at each pH and the observed rate constants were extrapolated to zero buffer concentration to correct for the influence of general acid and base catalysis on the hydrolysis rate. Experiments were carried out in duplicate with an uncertainty of ≤5%.

Solutions of 100 μM *p*-NPA were sonicated and analyzed in an identical fashion as *p*-NP. However, in the case of the *p*-NPA, the aliquots were adjusted to pH 7 by the addition of 0.2 mL of pH 7 buffer to 0.5 mL of sample. The samples were filtered and the absorbance at $\lambda = 272$ nm ($\epsilon = 8452$ M⁻¹ cm⁻¹) was measured. The contribution to the absorbance at 272 nm by *p*-NP ($\epsilon = 1777$ M⁻¹ cm⁻¹) was subtracted from the total absorbance. The use of methanol as a cosolvent was shown to substantially decrease the observed rate constant. Thus, no further experiments were done with this cosolvent. *p*-NPA dissolved in water after approximately 2 h of stirring and mild heating. The pH dependency of the reaction rate was established by a variation in buffer concentration or by using phosphoric acid. Ionic strength was varied with NaCl. NO₃⁻ and NO₂⁻ concentrations were determined by capillary electrophoresis (Dionex Capillary Electrophoresis System I) using a silica column (~60 cm) and a standard method for anion analysis.²⁴

Water with 18.2 mΩ resistivity (MilliQ UV Plus System) was used in the preparation of all aqueous solutions. *p*-NP and *p*-NPA (Aldrich, 99%+ and 97% purity, respectively) were used without further purification. Phosphoric acid, sodium chloride, and potassium phosphate monobasic were reagent grade and used without further purification.

Results and Discussion

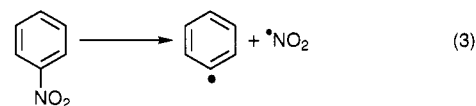
Comparative rate thermometry employing *p*-NP as a probe molecule can be used in order to estimate the effective temperatures achieved during bubble collapse.²⁵ *p*-NP¹ is a suitable probe molecule since its kinetics and mechanism of degradation are well understood. The primary step during the sonolytic degradation of *p*-NP has been shown to be¹



The activation energy for this pathway of degradation, which involves carbon–nitrogen bond cleavage, can be estimated from shock-tube studies of nitrobenzene decomposition.²⁵ The reaction rate constant for carbon–nitrogen bond cleavage in nitrobenzene has been determined to be

$$k = A \exp\{-E_a/RT\} \quad (2)$$

where $A = 1.9 \times 10^{15}$ s⁻¹ and $E_a/R = 33\,026$ K, and the stoichiometry is given by



Using these values for A and E_a/R , we can estimate the effective temperature of the cavitation bubble as follows:

$$T_{\text{eff}} = \frac{-E_a/R}{\ln\left(\frac{k}{A}\right)} = \frac{-33026}{\ln\left(\frac{k}{1.9 \times 10^{15}}\right)} \text{ [K]} \quad (4)$$

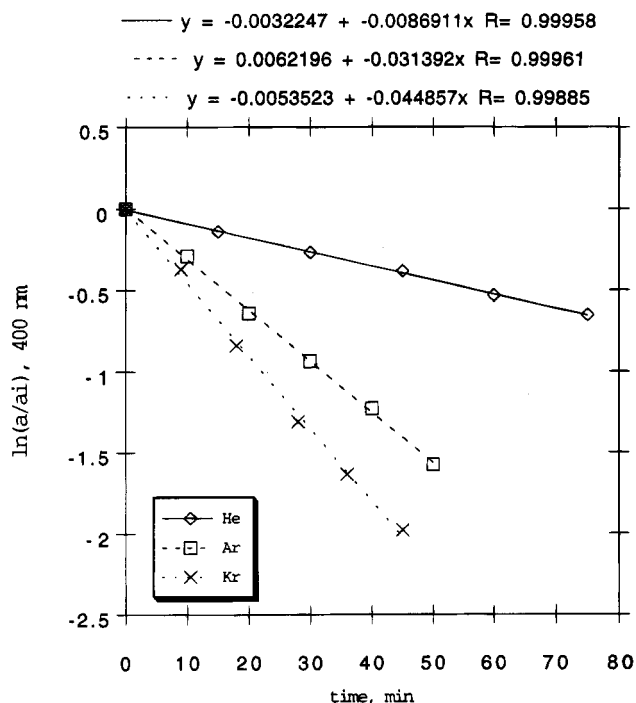
The relative temperature of bubble collapse can be adjusted by saturating the solution with gases characterized by substantially different specific heats, thermal conductivities, and solubilities. An important factor controlling bubble collapse temperature is the polytropic factor, K , of the saturating gas.⁹ From a knowledge of K we can estimate the maximum temperature obtained during bubble collapse from eq 5, where

$$T_{\text{max}} = T_0 \left\{ (K - 1) \frac{P_m}{P} \right\} \quad (5)$$

T_{max} is the temperature of bubble upon collapse, T_0 is the temperature of the bulk solution, P is the pressure in the bubble at its maximum size (i.e., the vapor pressure of the solvent), P_m is the pressure in liquid at moment of transient collapse, and $K = C_p/C_v$. The value of K is associated with the amount of heat released from the gas inside the bubble during adiabatic compression. As K increases, the heat released upon bubble collapse also increases. Additional physicochemical properties that may influence the temperature attained during bubble collapse include thermal conductivity, λ , and gas solubility. Values for the relevant physical properties^{26,27} of gases used in this study are listed in Table 1.

TABLE 1: Physical Properties of Selected Gases Used during Sonolysis^a

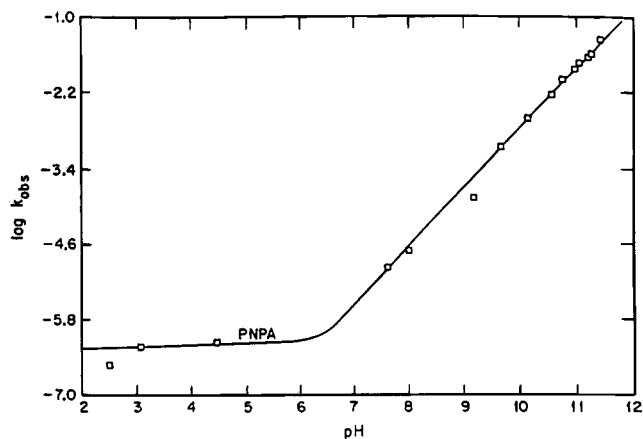
gas	polytropic index, κ	thermal conductivity, λ (mW/(mK))	solubility in water (m ³ /m ³)
Kr	1.66	17.1	0.0594
Ar	1.66	30.6	0.032
He	1.63	252.4	0.0086

^a At 600 K.**Figure 1.** First-order plot of *p*-NP degradation in a sonicated solution with different saturating gases. Rate constants in units of [s⁻¹]: (a) Kr: 7.5×10^{-4} , (b) Ar: 5.2×10^{-4} , (c) He: 1.4×10^{-4} . Also, a is the absorbance at 400 nm at time t after start of sonication, and a_i is the initial absorbance at 400 nm.**TABLE 2: Calculated Effective Temperature from Comparative Rate Thermometry with *p*-NP as Reacting System**

dissolved gas	rate const (s ⁻¹)	calcd temp (K)
Kr	7.5×10^{-4}	779
Ar	4.6×10^{-4}	772
He	1.2×10^{-5}	750

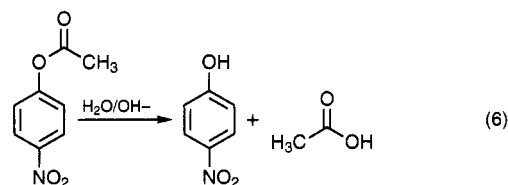
Thermal conductivities of the dissolved gases have been inversely correlated to sonoluminescence intensity²⁸ as well as with variable rates of free-radical formation^{29,30} during sonolysis. A low thermal conductivity favors high collapse temperatures because the heat of collapse will dissipate less quickly from the cavitation site. Highly soluble gases should result in the formation of a larger number of cavitation nuclei and more extensive bubble collapse since gases with higher solubilities are more readily forced back into the aqueous phase. Thus, a gas with both a low thermal conductivity and high water solubility should yield the highest temperature upon cavitation bubble collapse. On the basis of physical properties, we predict that krypton will yield the highest rate of *p*-NP degradation, while helium should yield the lowest relative rate.

The sonolytic degradation of *p*-NP is found to be a first-order reaction for all gases as shown in Figure 1. Using the rate constants obtained from this data and eq 3, we estimate the effective average temperatures at the interface of the collapsing bubbles for each gas (Table 2). The highest effective temperature is achieved in a Kr-saturated solution, whereas a

**Figure 2.** pH dependence of k_{obs} for the hydrolysis of *p*-NPA under ambient conditions.

He-saturated solution results in the lowest effective temperature, as predicted above. Although the value of K is similar for all three gases, helium has an unusually high thermal conductivity and a relatively low solubility in comparison to Ar and Kr. Thus, the difference in the resulting effective temperature is also larger than that between Ar and Kr.

Probing for Supercritical Water during Cavitation. Given the typical temperatures and pressures attained during bubble collapse, we postulate the existence of microscopic domains of supercritical water that are continuously variable in time and space. Because of the transient nature of the supercritical water phase, indirect methods are required to determine its existence in an ultrasonically irradiated system. Examination of reaction rate data in the context of activated complex theory (ACT) may give us some indication of a change in the reaction environment. The hydrolysis of *p*-NPA was chosen as a model reaction to probe for supercritical water at the bubble interface. The reaction most likely is accelerated in that region because the compound is not volatile and is relatively hydrophobic. Furthermore, the reaction does not involve hydroxyl radical and thus the interpretation of the observed reaction rate constants should not be complicated by formation rates of radicals produced during cavitation. Observed rate constants are highly pH dependent and range from 10^{-6} to 10^{-3} s⁻¹ in the pH range 2–10 for this reaction under ambient conditions (Figure 2). Above pH 6.5, the hydrolysis of *p*-NPA is base-catalyzed:



The rate law for *p*-NPA hydrolysis is written as

$$v = k_{\text{obs}}[p\text{-NPA}] = -d[p\text{-NPA}]/dt \quad (7)$$

where

$$k_{\text{obs}} = k_{\text{H}_2\text{O}}[\text{H}_2\text{O}] + k_{\text{OH}^-}[\text{OH}^-] + k_{\text{H}^+}[\text{H}^+] \quad (8)$$

with $k_{\text{H}^+} \approx 0$. The pH dependency of the control reaction is shown in Figure 2.

The overall first-order rate constant for *p*-NPA hydrolysis contains two terms that account for the uncatalyzed reaction with water and for the base-catalyzed pathway. Under normal conditions, the concentrations of the water and OH⁻ (at a

constant pH) remain constant and thus the overall rate constant is treated as a pseudo-first-order constant. The observed rate constants were found to be $k_{\text{H}_2\text{O}} = 6.0 \times 10^{-7} \text{ s}^{-1}$ and $k_{\text{OH}^-} = 11.8 \pm 0.5 \text{ M}^{-1} \text{ s}^{-1}$ and were determined from standard analysis of spectrophotometric data as a function of time.

The sonolytic acceleration of *p*-NPA hydrolysis has been reported previously by Kristol.³¹ He noted that several esters with widely different activation energies showed approximately the same relative enhancement in hydrolysis rates in the presence of ultrasound. Esters with substantially different activation energies for hydrolysis should show different relative rate enhancements, if these apparent enhancements were due only to the very high microscopic temperatures generated by cavitation bubble collapse. Our basic hypothesis, in this case, is that a change in the thermodynamics of the formation of the activated complex may account for changes in the observed reaction rates and reflect a change in either the microscopic environment and/or the mechanism. For a bimolecular reaction we can use the following activation parameters:

$$\Delta S^\ddagger = R(\ln A - \ln(k_{\text{B}}T/h) - 1) \quad (9)$$

$$\Delta H^\ddagger = E_a - RT \quad (10)$$

$$\Delta G^\ddagger = \Delta H^\ddagger - T\Delta S^\ddagger \quad (11)$$

to characterize the overall rate of reaction, where E_a is the intrinsic activation energy, A is the preexponential factor, $R = 8.31 \text{ J mol}^{-1} \text{ K}^{-1}$, $k_{\text{B}} = 1.38 \times 10^{-23} \text{ J K}^{-1}$, and $h = 6.626 \times 10^{-34} \text{ J s}$. E_a and A are determined experimentally from kinetic data.

The measured rate constant for hydrolysis of *p*-NPA at the bubble interface should be different from the rate constant determined from analysis of the bulk solution since the solution is not homogeneous. In order to determine a rate constant that is as close as possible to the intrinsic rate constant at the bubble interfaces, several other bulk solution parameters must be considered, including ionic strength, cosolvent effects, and pH.

Given that the interface between the hot gas in the bubble and the surrounding cooler liquid is hydrophobic,³² organic compounds will partition to that region much more effectively than ions. Thus, a variation in the ionic strength of the bulk solution should have a negligible influence on the hydrolysis rate constant. As shown in Figure 3, the observed hydrolysis rate constants do not vary appreciably over the range of ionic strength from 0.0 and 0.3 M.

Methanol, when used as a cosolvent can be present at a large excess compared to *p*-NPA. Under these conditions, methanol may preferentially accumulate at the bubble interface. In this way, a methanol cosolvent is predicted to slow down the rate of sonolysis of most organic molecules. This prediction is supported by the data shown in Figure 4 which provides a comparison of the rate constants observed in irradiated solutions in the absence (\diamond , \square) and presence (\times , $+$) of 0.25% (v/v) methanol. The rate constants are found to be significantly larger in solutions that were prepared without methanol.

Over a pH range of 3–8, the overall first-order rate constants are essentially invariant in a sonicated solution as shown in Figure 5. This pH dependency is consistent with the tendency for water in a dense supercritical state to have a higher ion activity product relative to normal-phase water; a higher value for K_{W} should result in a higher concentration of both OH^- and H^+ for a given set of conditions. Thus, we expect that the $k_{\text{OH}^-}[\text{OH}^-]$ term of k_{obs} (eq 8) should be enhanced significantly

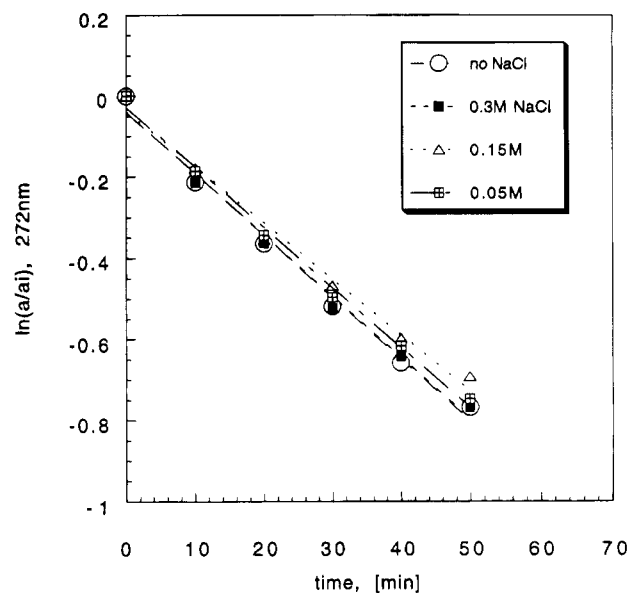


Figure 3. Effect of ionic strength on hydrolysis kinetics. Initial ester concentration, $[p\text{-NPA}]_i = 100 \mu\text{M}$.

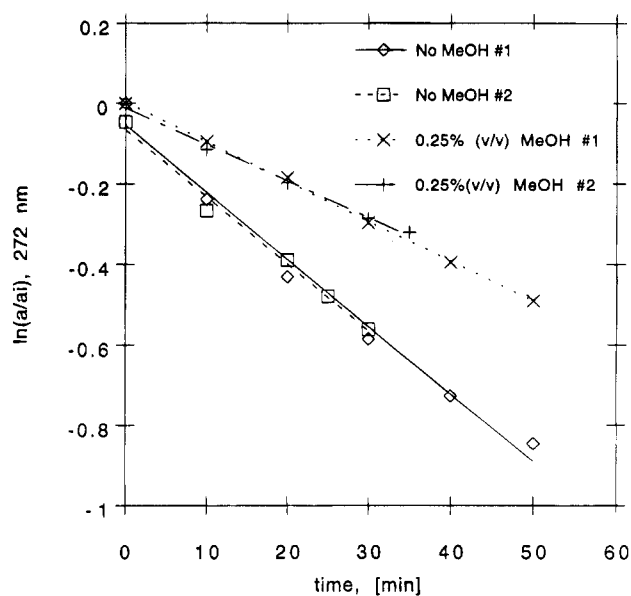


Figure 4. Effect of codissolved methanol on hydrolysis kinetics. Initial ester concentration, $[p\text{-NPA}]_i = 100 \mu\text{M}$.

in the presence of transient SCW. Selected properties of supercritical water and water under ambient conditions compared in Table 4.

The optimal set of conditions for determination of intrinsic rate constants proved to be an unbuffered solution of $100 \mu\text{M}$ *p*-NPA in the absence of a cosolvent. The amount of NO_2^- and NO_3^- produced during *p*-NPA sonolysis was insignificant. This indicates that the main reaction pathway for *p*-NPA was hydrolysis of the ester linkage rather than pyrolytic denitration of the nitro group. Figure 6 compares the relative values of k_{obs} in the presence of different saturating gases. The hydrolysis rate constants vary from 9.8×10^{-5} to $3.8 \times 10^{-4} \text{ s}^{-1}$, depending on the nature of the dissolved gas.

The Arrhenius plots for sonicated and unsonicated solutions are shown in Figures 7 and 8. Using the overall activation energies determined from these plots, the respective activation parameters can be calculated. As shown in Table 3, the activation free energy, ΔG^\ddagger , for hydrolysis appears to increase in the sonicated system compared to the unsonicated solution

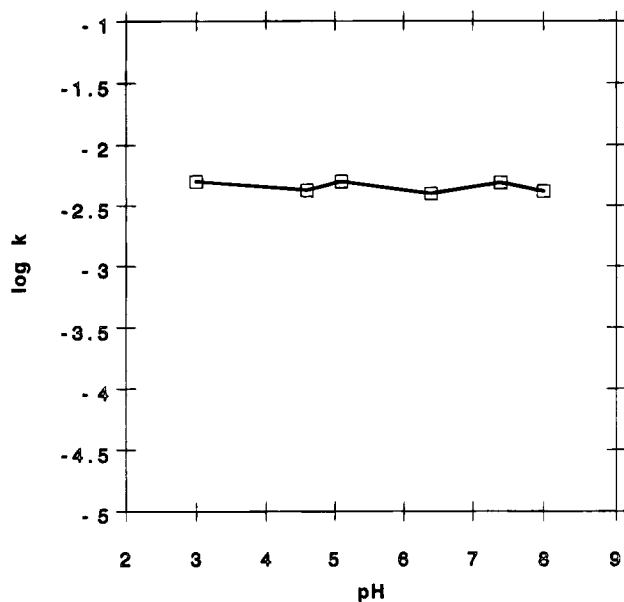


Figure 5. *p*-NPA hydrolysis rate constant as a function of pH.

TABLE 3: Thermodynamics of *p*-NPA Hydrolysis in Sonicated and Unsonicated Solutions^a

thermodynamic property	sonicated	unsonicated
ΔS^\ddagger	-47 J/(mol K)	-107 J/(mol K)
ΔH^\ddagger	211 kJ/mol	71.5 kJ/mol
ΔG^\ddagger	248 kJ/mol	155 kJ/mol

^a Quantities calculated using representative interfacial temperature of 780 K.

TABLE 4: Selected Properties of Different Phases of Water^a

physical state	ρ (g/mL)	ϵ	$\log K_w$ (mol ² /L ²)	μ (mPa/s)
supercritical	0.3	~6	-11.4 ^b	~10 ²
ambient	1	78.5	-14	~10 ³

^a At the critical point: $T_c = 647$ K, $P_c = 221$ bar. Under ambient conditions: $T = 298$ K, $P = 1$ bar. $\rho =$ density, $\epsilon =$ dielectric constant, $K_w =$ ion-activity product, $\mu =$ viscosity. ^b Calculated from equation in ref 17. All other values from ref 16.

primarily due to an increase in the value of ΔH^\ddagger . The higher value of ΔH^\ddagger in the sonicated system may result in part from its correlation with heat capacity which is a function of temperature. The heat capacity of water greatly increases in the supercritical regime¹³ and thus may contribute to an increase in ΔH^\ddagger during sonolysis. However, the corresponding reaction rate constant is also higher because of the net effect of an increasing effective reaction temperature. On the other hand, ΔS^\ddagger for hydrolysis appears to decrease in the presence of ultrasound. The apparent change in ΔS^\ddagger can be explained by considering changes in both the transition state and reactant interactions with the solvent, which are affected by the lower density and dielectric constant of the supercritical phase. Because the solute molecules are further apart in the supercritical domain, fewer are available for solvation of the polar transition state compared to the number which can cluster near the transition state in water at its normal density. In addition, the lower dielectric constant implies that when the organic solute is introduced into the supercritical phase, disruption of the solvent structure should be less compared to the disruption in the hydrogen bonds when an organic solute is introduced into liquid water.

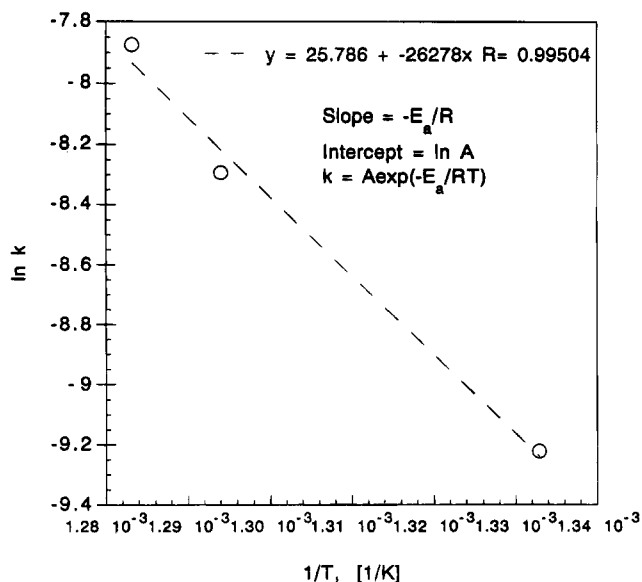


Figure 6. Arrhenius plot of hydrolysis rate constants of *p*-NPA in sonicated solution. Initial pH, pH_i = 6.1, initial ester concentration, $[p\text{-NPA}]_i = 100 \mu\text{M}$.

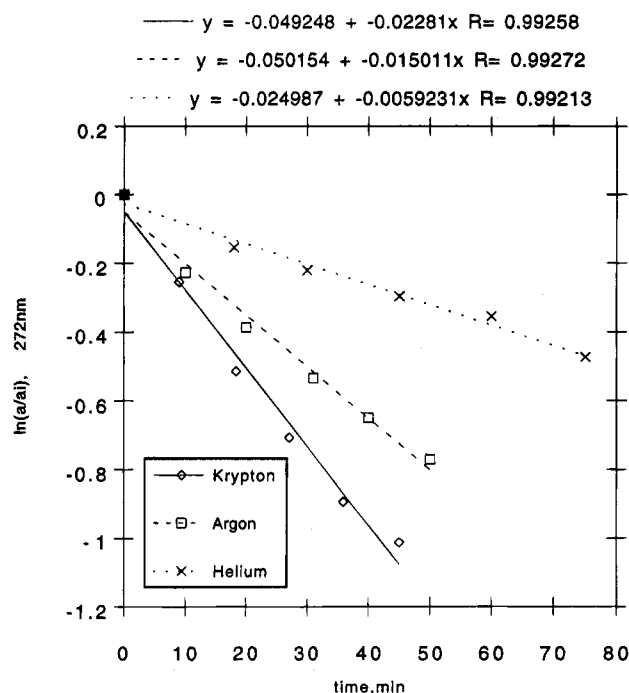


Figure 7. First-order plot of *p*-NPA hydrolysis in a sonicated solution with different saturating gases. Rate constants in units of $[\text{s}^{-1}]$: (a) Kr: 3.8×10^{-4} , (b) Ar: 2.5×10^{-4} , (c) He: 9.8×10^{-5} . Also, a is the absorbance at 272 nm at time t after start of sonication, and a_i is the initial absorbance at 272 nm.

Model for Formation of the Total Amount of Supercritical Water during Sonolysis

In light of the above results, we now proceed to estimate the fraction of an individual cavitating bubble, and total fraction of a cavitating solution, that is in the transient supercritical regime.

Flint and Suslick¹² and Sehgal et al.¹⁰ have clearly demonstrated that temperatures and pressures within a collapsing cavitation bubble exceed the critical point of water. On the basis of previously estimated temperatures within a collapsed bubble and a smaller layer of surrounding liquid,³³ we now attempt to describe the spatial and temporal temperature

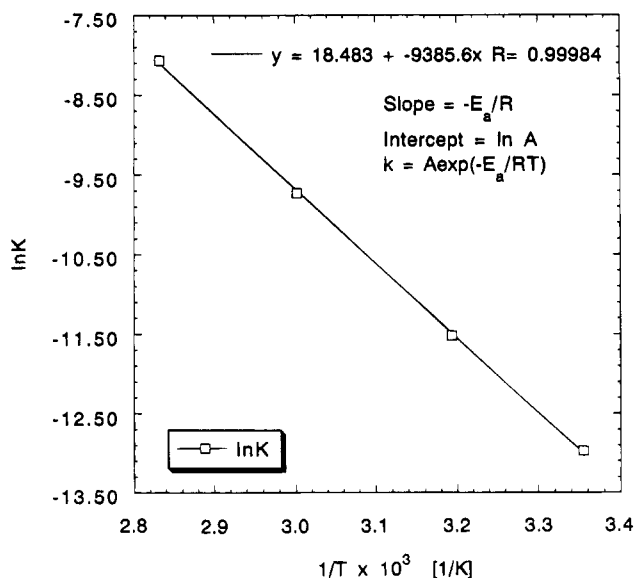


Figure 8. Arrhenius plot of hydrolysis rate constants of *p*-NPA in unsonicated solutions. Initial pH, pH_i = 6. Ionic strength, *I* = 0.4 M (NaCl). Initial ester concentration, [*p*-NPA]_i = 100 μM.

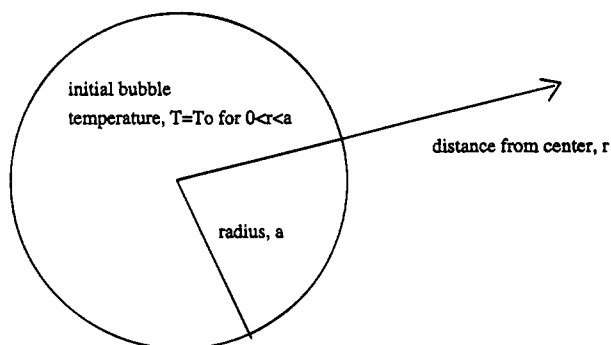


Figure 9. Schematic of the heat-transfer model with initial conditions.

distribution around a bubble just after its collapse. In order to obtain a simple first-order approximation of the heat transport from the interior of a hot bubble to the surrounding bulk liquid, we need to make several severe assumptions. Thus, we caution that this model should be viewed as a qualitative estimation rather than a precise description of the real physical phenomenon. Our goal is to show qualitatively that conditions occur around a collapsed bubble that are in accord with existence of supercritical water as suggested by our experimental results and to estimate the total volume of supercritical water present in a typical solution exposed to ultrasound.

The hydrodynamic life of the bubble before collapse is excluded from this analysis. Thus, we assume that the collapsed bubble is an instantaneous point source of heat embedded in an infinite matrix at ambient temperatures, as shown in Figure 9. Furthermore, we assume that conduction provides the only means of heat transfer, and thus we ignore heat transport by convection and radiation. We also assume that the bubble retains its spherical shape after collapse. The heat capacity, thermal conductivity, and density of the collapsed bubble are assumed to be the same as of the surrounding water at room temperature. In addition, we assume that a uniform temperature is attained within the bubble immediately after collapse.

The following values for the physical properties of liquid water at 303 K are used in the calculation. The heat capacity, C_p , 4178.4 J/(kg K), the thermal conductivity, λ , 0.6154 J/(s m K), and the density, ρ , 995.65 kg/m³, were taken from the *Handbook of Chemistry and Physics*.³⁴ The initial radius, a =

150 μm, and the initial temperature of the collapsed bubble, T_0 = 5000 K, have previously been estimated by Suslick.^{12,33} The temperature of the water surrounding the collapsed bubble, T_{med} , was 300 K.

Given all these assumptions, we can write the heat transport equation as

$$\partial T / \partial t = k \nabla^2 T \quad (13)$$

where the thermal diffusivity, k , in units of (m²/s) is given as $\lambda / (\rho C_p)$. The Laplacian, written in spherical polar coordinates

$$\nabla^2 = \frac{1}{r^2} \frac{\partial}{\partial r} \left[r^2 \frac{\partial}{\partial r} \right] + \frac{1}{r^2 \sin \theta} \left[\sin \theta \frac{\partial}{\partial \theta} \right] + \frac{1}{r^2 \sin^2 \theta} \frac{\partial^2}{\partial \phi^2} \quad (14)$$

can be simplified, since we have assumed that the collapsed bubble retains its spherical shape and that it has a uniform initial temperature T_0 . The resulting temperature distribution, $T(r)$, is, therefore, only a function of the distance from the bubble center and is independent of the angles θ and ϕ . With these assumptions we can write

$$\frac{1}{k} \frac{\partial T}{\partial t} = \frac{\partial^2 T}{\partial r^2} + \frac{2}{r} \frac{\partial T}{\partial r} \quad (15)$$

For the initial conditions, $T = T_0$, for $t = 0$, $0 < r < a$ and $T = T_{med}$, for $t = 0$, $r > a$ and the boundary condition $T = \text{finite}$, and for $r = 0$, the solution to eq 14 is given^{35,36} as

$$T_{red} = \frac{1}{2} \left[\operatorname{erf} \left(\frac{\frac{r}{a} + 1}{2 \left[\frac{k t}{a^2} \right]^{1/2}} \right) - \operatorname{erf} \left(\frac{\frac{r}{a} - 1}{2 \left[\frac{k t}{a^2} \right]^{1/2}} \right) \right] \dots \\ \dots - \frac{a}{r \sqrt{\pi} \left[\frac{k t}{a^2} \right]^{1/2}} \left[\exp \left(- \left(\frac{\frac{r}{a} - 1}{2 \left[\frac{k t}{a^2} \right]^{1/2}} \right)^2 \right) - \exp \left(- \left(\frac{\frac{r}{a} + 1}{2 \left[\frac{k t}{a^2} \right]^{1/2}} \right)^2 \right) \right] \quad (16)$$

where the error function is given by

$$\operatorname{erf}(x) = \frac{2}{\sqrt{\pi}} \int_0^x \exp[-y^2] dy \quad (17)$$

while the reduced temperature is defined as

$$T_{red} = \frac{T - T_{med}}{T_0 - T_{med}} \quad (18)$$

In eq 17 T_0 is the initial temperature of the collapsed bubble, T_{med} is the initial temperature of the surrounding water, and T_{red} is the reduced temperature as a function of the distance from the center of the bubble, r , at an elapsed time, t . The actual temperature can be calculated from the definition of the reduced temperature. In Figure 10 we show a plot of T_{red} vs r/a , obtained from the numerical solution of eq 15. The maximum radius of a shell around the collapsed bubble with a temperature exceeding the critical value $T_c = 647$ K can also be calculated for each given time interval after collapse. The times and corresponding reduced distances are given in Table 5. The estimated lifetime and spatial extent of the supercritical phase at a single cavitation site are on the order of milliseconds and micrometers. After 10 ms the radius of the supercritical

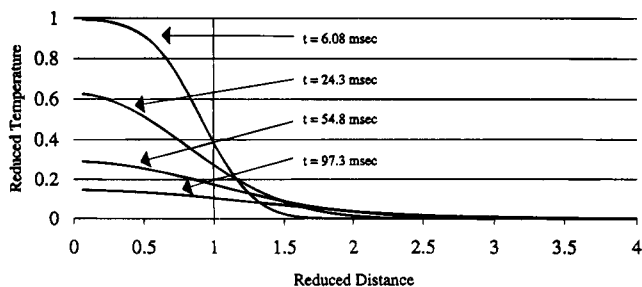


Figure 10. Plot of the reduced temperature, T_{red} , vs the distance from the center of the bubble, r , for various times after bubble collapse.

TABLE 5: Reduced Radii and Volumes of the Hot Layer Around a Collapsed Cavity and Corresponding Elapsed Times

i	time elapsed since collapse (ms)	reduced distance from center, $r(t_i)/a$, with $T > T_c$	vol of hot shell $V_{shell}(t_i)$ (pL)
0	0	1.000	0
1	1	1.147	7.2
2	2	1.200	10.3
3	5	1.307	17.4
4	10	1.400	24.7
5	15	1.467	30.5
6	30	1.573	40.9
7	50	1.613	45.2
8	70	1.573	40.9
9	90	1.467	30.5
10	110	1.307	17.4
11	120	1.200	10.3
12	130	1.067	3.04

region around a collapsed bubble extends about 40% farther into the bulk solution than the original cavity. The radius of the supercritical shell expands up to 160% of the original bubble radius at 50 ms after collapse.

We can also estimate the fraction of the total volume of a sonified aqueous solution that is actually in the supercritical state. The volume $V_{shell}(t_i)$ of the hot layer, where $T > T_c$, around a collapsed cavity can now be calculated as a function of time.

$$V_{shell}(t_i) = \frac{4}{3}\pi a^3 \left[\left(\frac{r(t_i)}{a} \right)^3 - 1 \right] \quad (19)$$

If N is the number of cavities that collapse per unit volume per unit time, the fraction of the aqueous solution that is in the supercritical state, x_{scw} , is given as

$$V_{scw}/V_{total} \equiv x_{scw} = N \sum_i V_{shell}(t_i) [t_i - t_{i-1}] \quad (20)$$

The number density of nuclei and their size distribution has been measured by Katz and Acosta.³⁷ However, there are no experimental data for the number density of nuclei or actual cavitation bubbles in water during ultrasonic irradiation. Suslick and Hammerton¹⁴ give an estimate for the number of collapsing bubbles per time and volume. If we use their estimate of $N = 4 \times 10^8 \text{ s}^{-1} \text{ m}^{-3}$, we determine that $x_{scw} = 0.0015$.

Our simple model predicts that approximately 0.15% of the irradiated water is in the supercritical state at any point in time. Depending on the extent to which supercritical water accelerates chemical reactions, this fraction may represent a substantial contribution to reaction rate enhancements that have been reported previously for chemical reactions in the presence of ultrasound.

Conclusions

p-NPA hydrolysis is an ultrasonically irradiated solution exhibits an observed rate constant which is enhanced by about 2 orders of magnitude in comparison to the same hydrolysis under ambient conditions at 25 °C. Furthermore, k_{obs} is found to be relatively insensitive to the solution pH in the presence of ultrasound while k_{obs} under ambient conditions is a strong function of pH, i.e., $k_{obs} = k_0 + k_{OH^-}[\text{OH}^-]$. The latter result is distinct from that observed in unsonified solutions and suggests that the reaction rate enhancement occurs at the cavitation bubble interface. Both the enhanced hydrolysis rate and its pH independence may be explained by the existence of supercritical water around the collapsing cavitation bubbles. Hydrolysis may be accelerated, in part, by a higher concentration of OH^- at the hot bubble interface, which results from the higher ion product, K_w , of SCW. The apparent decrease of ΔS^\ddagger in the presence of ultrasound suggests that the rate enhancement might be due to a physical change in the microscopic environment surrounding the substrate. In addition to our experimental evidence, a simple heat-transfer model predicts that approximately 0.15% of the irradiated water is in the supercritical state at any point in time, giving further evidence for the proposed existence of SCW in cavitating aqueous solutions. On the basis of these experimental findings and our semiquantitative calculations, we argue that supercritical water represents a potentially important component of sonochemistry, in addition to the free-radical reactions and thermal/pyrolytic effects¹⁻³ that have been demonstrated previously.

The existence of the SCW phase during acoustic cavitation has significant implications for hydrolysis reactions of environmental interest. Because the reaction occurs at or close to the bubble/water interface, compounds more hydrophobic than *p*-NPA are expected to exhibit even higher hydrolysis rate enhancements because the compound that is concentrated around the bubble will, once the bubble collapses, be embedded in supercritical water. The sonolysis of parathion at 25 °C results in complete hydrolysis within 30 min,³ whereas at 20 °C and pH 7.4 the noncatalyzed hydrolysis has a half-life of 108 days.³⁸

Finally, the existence of the supercritical phase in an ultrasonically irradiated solution suggests a modification of the conventional view of the reactive area at a cavitation site. This region is normally considered to consist of two discrete phases: a high temperature, low-density gas phase, and a more condensed and lower temperature liquid shell. An alternative description would include a structural change of the collapsing bubble due to the existence of SCW with properties more characteristic of water vapor than liquid water. The presence of SCW in a collapsing bubble may help to explain the observed fragmentation of a single bubble into a bubble cloud consisting of many smaller bubbles.³⁹

The application of SCW oxidation to wastewater treatment has been investigated in recent years.²¹⁻²³ One drawback of the large scale application of SCW oxidation is the inherently aggressive nature of water in the supercritical state, which results in extensive corrosion of reaction vessels. Corrosion of the reactor chamber lessens the economic feasibility of this method. We believe that the treatment of hazardous organic compounds with ultrasound could be a possible alternative to oxidation processes in bulk supercritical water. Due to the local confinement of supercritical water as generated during the collapse of gas cavities, the bulk solution remains at ambient pressures and temperatures, thus avoiding extensive damage to the reaction vessel.

Acknowledgment. The authors are grateful to EPRI (contract No. RP8003-36) and ARPA (Grant No. NAV 5HFMN

N0101492J1901) for generous financial support. We appreciate the support and encouragement of Drs. Ira Skurnick and Myron Jones and the helpful discussions provided by Professor Kenneth Suslick.

References and Notes

- (1) Kotronarou, A.; Mills, G.; Hoffmann, M.R. *J. Phys. Chem.* **1991**, *95*, 3630–3638.
- (2) Kotronarou, A.; Mills, G.; Hoffmann, M. R. *Environ. Sci. Technol.* **1992**, *26*, 2428–2430.
- (3) Kotronarou, A.; Mills, G.; Hoffmann, M. R. *Environ. Sci. Technol.* **1992**, *26*, 1462–1469.
- (4) Petrier, C.; Micolle, M.; Merlin, G.; Luche, J. L.; Reverdy, G. *Environ. Sci. Technol.* **1992**, *26*, 1639–1642.
- (5) Wu, J. M.; Huang, H. S.; Livengood, C. D. *Environ. Prog.* **1992**, *11* (3), 195–201.
- (6) Lord Rayleigh, *Philos. Mag.* **1917**, *34*, 94–98.
- (7) Noltingk, B. E.; Neppiras, E. A. *Proc. Phys. Soc. B* **1950**, *63B*, 674–685.
- (8) Noltingk, B. E.; Neppiras, E. A. *Proc. Phys. Soc. B* **1951**, *64B*, 1032–1038.
- (9) Mason, T.; Lorimer, J. *Sonochemistry: Theory, Applications, and Uses of Ultrasound in Chemistry*; Ellis Norwood, Ltd.: New York, 1988.
- (10) Sehgal, C.; Steer, R. P.; Sutherland, R. G.; Verrall, R. E. *J. Chem. Phys.* **1979**, *70* (5), 2242–2248.
- (11) Flint, E. B.; Suslick, K. S. *J. Am. Chem. Soc.* **1989**, *111*, 6987–6992.
- (12) Flint, E. B.; Suslick, K. S. *Science* **1991**, *253*, 5026, 1397–1399.
- (13) Gutiérrez, M.; Henglein, A.; Fischer, Ch.-H. *Int. J. Radiat. Biol.* **1986**, *50*, 313–321.
- (14) Suslick, K. S.; Hammerton, D. A. *IEEE Trans Ultrasonics Ferroelec Freq. Contr.* **1986**, *UFCC-33*, *2*, 143–147.
- (15) Gutiérrez, M.; Henglein, A.; Ibañez, F. *J. Phys. Chem.* **1991**, *95*, 6044–6047.
- (16) Shaw, R. W.; Brill, T. B.; Clifford, A. A.; Ecker, C. A.; Franck, E. U. *Chem. Eng. News* **1991**, *69* (51), 26–39.
- (17) Marshall, W. L.; Franck, E. U. *J. Phys. Chem. Ref. Data* **1981**, *10*, 295–304.
- (18) Li, L. L.; Egiebor, N. O. *Energy Fuels* **1992**, *6*, 35–40.
- (19) Lee, D. S.; Gloyna, E. F. *Environ. Sci. Technol.* **1992**, *26*, 1587–1593.
- (20) Klein, M. T.; Mentha, Y. G.; Torry, L. A. *Ind. Eng. Chem.* **1992**, *31*, 182–187.
- (21) Townsend, S. H.; Abraham, M. A.; Huppert, G. L.; Klein, M. T.; Paspek, S. C. *Ind. Eng. Chem. Res.* **1988**, *27*, 143–149.
- (22) Yang, H.; Eckert, C. A. *Ind. Eng. Chem. Res.* **1988**, *27*, 2009–2014.
- (23) Thornton, T. D.; LaDue, D. E., III; Savage, P. E. *Environ. Sci. Technol.* **1991**, *25*, 1507–1510.
- (24) Harrold, M. P.; Wojtusik, M.; Riviello, J.; Henson, P. *J. Chromatogr.* **1993**, *640*, 463–471.
- (25) Tsang, W.; Robaugh, D.; Mallard, G. W. *J. Phys. Chem.* **1986**, *90*, 5968–5973.
- (26) Kaye, G. W. C.; Labye, T. H. *Tables of Physical and Chemical Constants and Some Mathematical Functions*, 14th ed.; Longman Group Ltd.: London, 1973; p 54.
- (27) Braker, W.; Mossman, A. *Gas Data Book*, 6th ed.; Matheson Gas Products Inc.; 1980.
- (28) Young, F. R. *J. Acoust. Soc. Am.* **1976**, *60*, 100–104.
- (29) Kondo, T.; Kirschenbaum, L. J.; Kim, H.; Riesz, P. *J. Phys. Chem.* **1993**, *97*, 522–527.
- (30) Makino, K.; Mossoba, M. M.; Riesz, P. *J. Phys. Chem.* **1983**, *87*, 1369–1377.
- (31) Kristol, D. S.; Klotz, H.; Parker, R. C. *Tetrahedron Lett.* **1981**, *22*, 907–908.
- (32) Henglein, A.; Kormann, C. *Int. J. Radiat. Biol.* **1985**, *48*, 251–258.
- (33) Suslick, K. S.; Hammerton, D. A. Cline, Jr. R. E., *J. Am. Chem. Soc.* **1986**, *108*, 5641–5642.
- (34) *Handbook of Chemistry and Physics*, 71st ed., CRC Press: Boca Raton, FL, 1990.
- (35) Crank, J. *The Mathematics of Diffusion*, 1st ed.; Clarendon Press: Oxford, U.K., 1956.
- (36) Carslaw, H. S.; Jaeger, J. C. *Conduction of Heat in Solids*, 2nd ed.; Clarendon Press: Oxford, U.K., 1959.
- (37) Katz, J.; Acosta, A. *Appl. Sci. Res.* **1982**, *38*, 123–132.
- (38) Faust, S. D.; Goma, H. M. *Environ. Lett.* **1972**, *3*, 171–201.
- (39) Neppiras, E. A.; Coakley, W. T. *J. Sound Vibration* **1976**, *45*, 341–373.

JP941776N